Environ. Sci. Technol. **2005**, *39,* 8008−8013

Soot Emissions from Spherical Droplet Flames for Mixtures of JP8 and Tripropylene Glycol Monomethyl Ether

JUN H. BAE AND
C. THOMAS AVEDISIAN*
Sibley School of Mechanical and Aerospace Engineering, Cornell University, Ithaca, New York 14853-7501

The combustion of JP8 (a kerosene-based fuel) mixed with up to 20% (volume) tripropylene glycol monomethyl ether (TPGME, $CH_3[CH_2CH(CH_3)O]_3OH$) is studied to examine the influence of composition on soot dynamics for the configuration of an isolated and stationary droplet burning with nearly spherical symmetry. The spherical droplet flame is characterized by a one-dimensional transport process with a concentric flame and droplet, and a sooting configuration for which the soot aggregates are trapped between the droplet and flame in a "shell" or "cloud". Sooting tendencies are inferred from photographic documentation of the droplet burning process and are found to be in the approximate order JP8 > JP8 + 10% TPGME > JP8 + 20% TPGME. At 20% the soot cloud all but disappears. The maximum soot aggregate diameter is 80 (±17) nm, independent of composition. Preferential vaporization is pronounced as evidenced by a plateau in the evolution of the droplet diameter (squared) which indicates a dominant influence of TPGME over other constituents in JP8 that makes JP8/TPGME behave almost like a binary mixture despite the highly multicomponent nature of the JP8/TPGME blend. A scaling relationship for flame, soot cloud, and droplet diameters is shown to consolidate the measurements onto a single curve.

Introduction

The most widely used fuels in power and propulsion systems for military and commercial transport systems are kerosene derivatives. JP8 in particular is a multicomponent blend composed of no less than 200 constituents (*1*, *2*) that have a wide variety of boiling points, heats of vaporization, and sooting tendencies. Due to variability in the crude source, the composition of JP8 is not unique (*3*). [The variability of JP8 composition complicates interpretation and comparison of results from among different groups. Efforts have recently begun (*1*, *4*) to address this issue by proposing that transportation fuels (of which JP8 is one) be modeled by a select group of six chemical classes that would replicate most of the performance metrics of interest to power and propulsion systems. The concentrations of species in such a "surrogate" fuel have not yet been determined.]. On average, JP8 contains up to 25 vol % aromatics (*5*), which makes it a difficult fuel to burn without forming soot. In the current climate of high reliance on foreign sources of oil and concerns for environmental pollution, methodologies to reduce soot formation are important to develop. Interestingly, considerable effort has been devoted to improving JP8 for the noncombustion uses it serves, for example, to make it a more thermally stable coolant (*6*, *7*), though little has been written about reducing soot formation through the influence of additives (*8*, *9*).

The easiest way to influence combustion performance is through the use of additives. Those that contain bound oxygen ("oxygenated" compounds such as methanol) can be especially effective (*10*−*13*). The effect of oxygen on soot is chemical or physical: chemical, through attack of OH radicals on soot precursors such as C_2H_2 (*14*, *15*); physical, through a simple dilution effect. The influence can be substantial. For example, Miyamoto et al. (*11*) found that blending diesel fuel with oxygenate concentrations of 25−30% by mass produced significant reductions in particulate matter. Curran et al. (*12*) reported a reduction of emissions by over 80% for diesel fuel heavily diluted with methanol, but at an unrealistically high loading of 82%. Similarly, blends of JP8 and hexanol resulted in significant reduction of soot, also at high loading (50%) (*8*). At the same time, these effects on soot formation can come at the expense of other performance metrics such as fuel consumption, power output, and losses in engine boost (*13*).

Published results suggest that certain aspects about soot formation have a universal character which can be revealed by laboratory-scale experimentation, such as maximum primary particle size and soot inception temperature (see, e.g., refs *16* and *17*). The mechanism of converting fuel molecules to soot comes from a series of common steps for different combustion configurations. Fuel molecules pyrolyze and produce fuel intermediates (e.g., acetylene) that lead to "precursor" species (*18*) which are then converted to soot by a carbonization process when the temperature exceeds a critical value, generally on the order of 1350 K (*17*). Soot aggregates can grow by surface reactions with gaseous precursors and polycyclic aromatic hydrocarbons (PAHs) as well as by coagulation and coalescence.

Viable additives to JP8 for reducing soot would essentially attack the precursors during combustion. Molecules with bound oxygen are attractive for this purpose. They should be miscible in JP8 for ease of preparation and transport. Methanol is not a good choice for this reason; ethanol addition to JP8 poses complications for the experimental arrangement used in this study through its potential for microexplosions (*19*). Of the many oxygenates evaluated in their engine tests, Gonzalez et al. (*10*, *13*, *20*) studied a range of compounds with different molecular structures including ether, ester, and alcohol groups. Of the mono-, di-, and tripropylene glycol monomethyl ethers examined, tripropylene glycol monomethyl ether (TPGME, $CH_3[CH_2CH(CH_3)O]_3OH$) was found to be the most promising for future engine testing to reduce particulate matter (*10*, *13*, *14*, *20*), in that a 50% reduction of soot formation was observed for TPGME with 7% oxygen content by weight in diesel fuel (*10*).

In the present study we examine in greater detail the effect of TPGME from a more fundamental perspective than tests in a full-scale engine environment can create. We report on the influence of TPGME on soot dynamics using a well-characterized and simplified transport configuration. Recognizing that the vast majority of propulsion systems (e.g., engines) introduce fuels into the combustion chamber as a spray, of which droplets are the component elements, the most basic possible configuration is an isolated droplet burning in a quiescent ambience of air at atmospheric

* Corresponding author phone: (607) 255-5105; fax (607) 255-1222; e-mail: cta2@cornell.edu.

10.1021/es048516w CCC: $30.25

Published on Web 09/10/2005

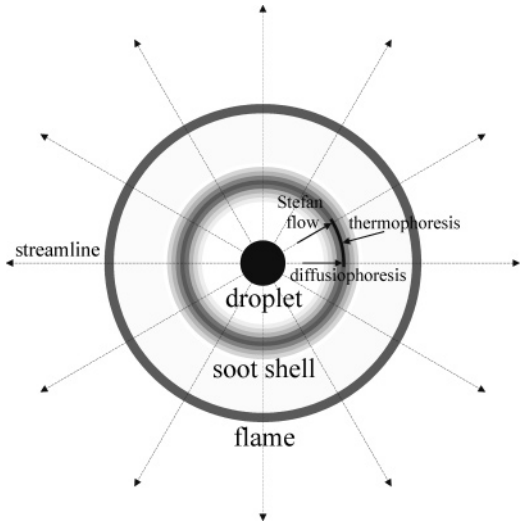

FIGURE 1. Schematic of idealization of spherically symmetric droplet burning with soot formation. The soot shell will achieve the position appropriate for the forces acting on the soot aggregates, being principally thermophoresis (inward) and evaporation-induced drag (outward).

pressure and temperature. Figure 1 illustrates the configuration of interest here (*21*−*23*).

The droplet and flame are spherical and concentric. Soot aggregates form on the fuel-rich side of the flame and are trapped in a sort of metastable equilibrium to form a "shell" or "cloud" where the forces on them balance, being principally the outwardly directed drag associated with the evaporation-induced velocity and the inwardly directed thermophoretic force associated with the temperature gradient between the droplet and flame. Streamlines of the flow ideally resemble the spokes of a wheel because gas transport is purely in the radial direction. These features combine to make the idealization in Figure 1 a "canonical" configuration for droplet combustion. Our idea to subject a complex fuel such as JP8 and its mixtures with TPGME to the environment of Figure 1 is an attempt to exploit these attributes and to provide data useful for modeling complex combustion aspects such as the influence of radiation and soot formation on droplet burning (*24*, *25*).

As burning progresses, the soot aggregates accumulate and the cloud becomes more dense. Particularly large aggregates may drift out of the shell toward the flame (*23*) where they can oxidize (*21*, *26*, *27*) because of small perturbations in the flow, caused, for example, by a physical drifting of the droplet as it burns. The experimental apparatus is specifically designed to exclude this sort of transport by restricting motion of the droplet.

The geometry of Figure 1 is not in any way intended to mimic conditions in a real combustor. Rather, the goal is to bring a fundamental perspective to combustion of JP8 and its blends with TPGME. The relationship between the isolated case in Figure 1 and the situation experienced by droplets in a practical engine environment is through subgrid models in spray codes that track the behavior of individual droplets (*28*). The consistency of correlations that correct for convection in these subgrid models is dependent on recovering the one-dimensional limit of zero convection, which is the case depicted in Figure 1.

The compositions examined are those found to be important in engine combustion studies, namely, 20 and 10 vol % (*10*, *20*), corresponding to 7.2% and 3.7% oxygen content. Specific aspects examined include the evolution of the droplet, flame, and soot dynamics, how blending with TPGME influences these quantities, and the overall sooting

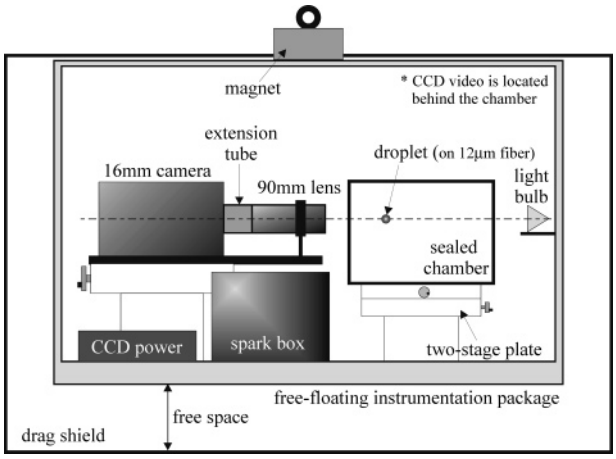

FIGURE 2. Schematic of the experimental package that is physically dropped to create low gravity and low convection. The outer chamber shields the inner package from air drag, which thereby lowers the convection level and provides for a more spherically symmetric burning configuration.

propensities of JP8 and TPGME. Quantitative measurements include the evolution of droplet (D), flame (D_f), and soot cloud (D_s) diameters to give information on the burning rate and unsteady behavior, which are important parameters for modeling. We also define an index that measures the tendency to soot and compare it among the JP8/TPGME compositions examined. Droplets with initial diameters in a relatively tight range of 400−500 μm diameters were examined to eliminate the effect of the initial droplet diameter on soot formation (*29*, *30*). This size range is much larger than that of droplets in practical sprays, which are typically under 100 μm diameter. The smallest dimension we can resolve is about 30 μm. If we were to start with a 100 μm droplet, we would be able to track 70% of its burning history, while for a 500 μm droplet we can track 94% of the burning history. Droplets of 500 μm diameter also exhibit features similar to those of their smaller counterparts, yet they allow for higher average optical quality.

Experiment

General Procedure and Materials. Spherical droplet flames are promoted by performing the experiments at low gravity to eliminate the influence of convection. Gravity levels are less than 10^{-4} of the earth's gravity (9.8 m/s^2), which provides sufficiently low Rayleigh numbers that the flame was nearly spherical. The experiments are conducted in a free-fall facility that provided 1.2 s of low gravity. This time is adequate to observe the complete burning history for the sub-millimeter-sized droplets examined (*31*, *32*). The general procedure of the experiments is to first deploy a test droplet in its sealed surroundings and then to put the confined droplet and hardware shown in Figure 2 into free-fall, with two cameras viewing the burning history in perpendicular directions. During the downward flight of the instrumentation package, the droplet is ignited and the burning process recorded photographically. Details of the experimental design and procedures are given in ref *33*. The JP8 and TPGME used in this study were supplied by Southwest Research Institute (San Antonio, TX).

Droplet Deployment and Ignition. Test droplets are anchored on very thin SiC fibers, 12 μm diameter, using a previously developed design for supporting droplets (*8*, *34*). Two SiC fibers are placed across four posts in a crossing pattern with the droplet mounted at the intersection of the fibers. The fibers are crossed at an angle of 120° so that the glow from the fiber associated with the interaction of the fiber with the flame would not obscure any portion of the

droplet or soot cloud that formed. Unlike free-droplet techniques, the fiber may influence combustion through heat conduction along the fiber, the droplet and flame shapes, and the geometries of the soot patterns that form (see refs *35* and *36*). Since measurements of the supported droplets compared very favorably with a droplet burning in a free-floating mode (evolution of the droplet diameter) (*8*), we assumed that the fiber did not exert an influence on the burning rate. We did notice some distortion of the soot cloud late in the droplet burning lifetime, though the unusual patterns of soot trapping associated with very large fiber supports (*36*) never arose.

Droplets are mounted on the fibers by essentially "shooting" a droplet formed from a piezoelectric generator (e.g., similar to an inkjet generation method (*31*)) at the intersection of the two fibers. The droplet is ignited by two adjustable sparks (spark duration of 0.8 ms) positioned on opposite sides of the droplet. The electrodes are then immediately retracted away from the droplet. The sparks are activated 320 ms after the period of low gravity commences to allow vibrations to subside that are commonly caused by the physical separation of the instrumentation package from the magnet that holds the package in place prior to dropping. This manner of ignition is designed to promote ignition symmetry. Though it is completely different from what droplets would experience in a realistic engine environment, as noted previously our intention is not to simulate a practical liquid fueled burning situation but rather to create the idealized spherical configuration of Figure 1, and this manner of ignition was favorable to that end.

Data Acquisition and Processing. For recording droplet and soot shell images, constant-intensity backlit images are taken using a GE ENG 150 W bulb for illumination and Eastman Kodak 7278 black and white film (ASA 125) with a LOCAM high-speed 16 mm movie camera operating at 200 frames/s. The camera is fitted with an Olympus 90 mm Zuiko lens and 100 mm extension tube (an aperture of f4.0 and a shutter speed of 1/450 s). The high-intensity backlighting was effective for observing the droplet through the dense soot cloud. Using a COHU 8295 camera with a Bausch & Lomb 48 mm 0.08 objective lens and an 80 mm extension tube, self-illuminated (i.e., nonbacklit) CCD color video images are also recorded for flame analyses.

Quantitative measurements of D and D_s are made by scanning each image from the 16 mm movie sequence into a PC (with a Microtex scanner at 3900 × 3900 dpi resolution) for analysis by Media Cybernetics ImagePro Plus 4.0 software. Corrections for slight asymmetry in the droplet shape due to the fiber are made by defining an equivalent diameter from the measured cross-sectional area of droplets. Soot shell diameters are taken from the diameter of a circle that best fits a user-defined periphery of the soot cloud. Measurement of D_s is begun when the soot cloud is clearly visible as a shell, and measurements are terminated when the soot shell aspect ratio becomes less than 0.9. The outer luminous zone is defined as the flame diameter, and it is obtained from video images displayed on a monitor using a video caliper. More detailed discussion of the measurement and analysis procedure is given elsewhere (*33*).

A semiquantitative assessment of the relative amount of soot formed for the various mixtures examined is made by defining an "apparent soot index" (ASI) as the ratio of the darkest areas surrounding a droplet (dark areas are due to soot) for JP8/TPGME blends relative to that of "pure" JP8:

$$\text{ASI} \equiv \frac{\text{area of the dark region around the TPGME/JP8 mixture droplet}}{\text{area of the dark region around the pure JP8 droplet}} \quad (1)$$

(i.e., ASI = 1 for JP8). The dark areas are identified by ImagePro Plus software and combined according to eq 1. Although this is an arbitrary definition as it considers soot visible in only one plane, it provides more quantitative judgments of soot formation compared to a simpler visual inspection of photographic image intensity.

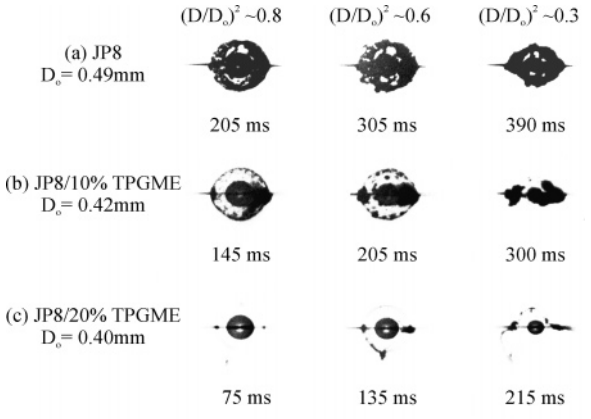

FIGURE 3. Selected backlit photographs of (a) JP8, (b) JP8/10% TPGME, and (c) JP8/20% TPGME droplets burning in air. The backlight intensities are identical. Note that the soot cloud is barely visible for (c).

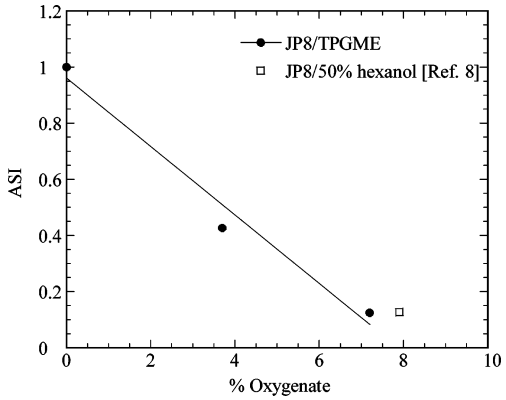

FIGURE 4. ASI of JP8/TPGME blends (TPGME 0%, 10%, and 20% in volume).

Soot aggregates are acquired from deposits on the support fibers at the end of the burning process and then analyzed using a LEO 922 energy-filtering transmission electron microscope which utilizes Koehler illuminations for superior digital image contrast. The aggregates sampled in this way correspond to the very end of the burning process. Mean aggregate "diameters" are extracted from transmission electron microscopy (TEM) negatives using the aforementioned image analysis software. The soot samples were prepared for TEM analysis by crushing them into finer-sized specimens using a mortar and pestle for a uniform specimen thickness over a large area. The soot specimens were attached to a copper-grid film 1/8 in. in diameter (SPI Supplies, model no. 3330C, Formvar on 300 mesh) with 2-propanol solvent and then mounted in the TEM instrument.

Results and Discussion

Flame and Soot Cloud Structure. Figure 3 illustrates the development of the soot cloud with selected black and white photographs using intense backlighting for JP8 (Figure 3a), JP8 + 10% TPGME (Figure 3b), and JP8 + 20% TPGME (Figure 3c) droplets. The three sets of photographs were selected to correspond to $(D/D_0)^2$ of 0.8, 0.6, and 0.3. The time after ignition is indicated beneath each photograph. The second photograph of each set happened to correspond to the most intense (i.e., darkest) image for that set as determined by the

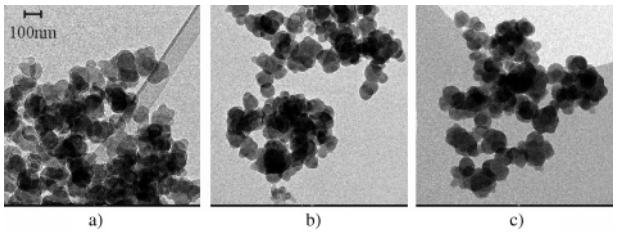

FIGURE 5. TEM images of soot aggregates collected at the end of burning: (a) JP8, (b) JP8/10% TPGME, (c) JP8/20% TPGME.

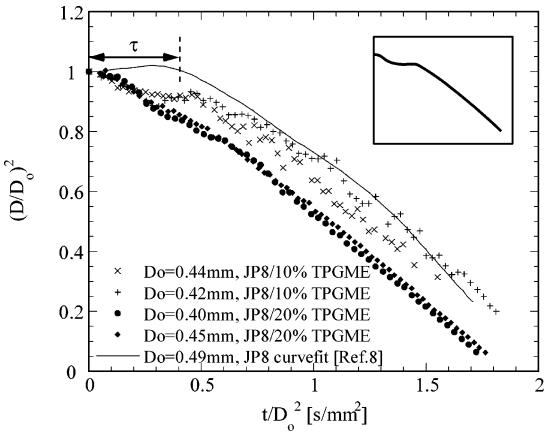

FIGURE 6. Evolution of the droplet diameter for both JP8/TPGME mixtures (10% and 20%). The initial heating period of the JP8 droplet is marked as "τ". The trend line in the inset illustrates the preferential vaporization of the JP8/10% TPGME mixture.

software analysis. With high-intensity backlighting, the droplet and soot are both visible for JP8 and JP8 + 10% TPGME. Some obscuration of the droplet is evident at later times due to soot accumulation in the shell for JP8, which decreases with increasing TPGME concentration. At 20%, the soot shell is not visible at all. This shows the influence of oxygen in TPGME on mitigating the formation of soot precursor species as noted previously.

Assuming that a less dense soot cloud implies less soot formed, the sooting propensities according to Figure 3 are in the order JP8 > JP8/10% TPGME > JP8/20% TPGME. This trend is consistent with the ASI shown in Figure 4, which also includes measurements from ref *8* for a JP8/50% hexanol (7.9% oxygen content) blend for comparison. The line drawn is meant to illustrate the trend.

At later times in Figure 3, soot deposits can be seen on the fiber. These were extracted from the fiber and analyzed by TEM. Figure 5 shows TEM images of soot aggregates for JP8 and JP/TPGME blends. The aggregates appear to have a somewhat spherical or elliptical shape which is consistent with previous work on a different flame geometry (*16*). However, while the mean aggregate size (calculated as the arithmetic mean of the transverse and longitudinal lengths) is about 80 (±17) nm and is independent of concentration, the aggregate size is considerably larger than that of the soot precursors reported in buoyancy-dominated flames (*16*). The trend of larger aggregate size with reduced convection level is consistent with prior observations (*37*).

It is common practice to define a flame "standoff" ratio as the relative position of the flame to the droplet diameter, D_f/D, and similarly for the soot shell, D_s/D. The local droplet diameter that is used to form these ratios is shown in Figure 6 for both 10% and 20% TPGME in which the data are presented in coordinates of the classical theory of spherically symmetric droplet combustion (see, e.g., ref *18*). Comparatively high scatter in the data of the 10% TPGME mixture is the result of soot obscuration of the droplet image. On the other hand, the data quality of the 20% TPGME mixture is higher because of reduced soot formation (Figure 3c). For comparison to pure JP8, data from ref *8* are included in Figure 6 (curve-fit line).

Mixture Effects. Two noticeable features of the addition of TPGME are as follows. First, an initial heating period for JP8 (spanning the time range of τ labeled in Figure 6) was significantly decreased by the addition of TPGME (both 10% and 20% concentrations). This reduction is the result of a higher thermal diffusivity of TPGME relative to JP8 which produces a smaller thermal penetration depth (*28*) for TPGME relative to JP8. Second, preferential vaporization is observed for both TPGME mixtures, even though pure JP8 did not show evidence of preferential vaporization even with its multicomponent nature.

The inset in Figure 6 is an idealization of preferential vaporization. It is typically considered to be due to a volatility difference between components in a multicomponent fuel blend in which the most volatile species evaporates and leaves behind the second component or additional components, which then evaporate sequentially. A flat transition zone ("plateau") is the result of compensating the reduction of liquid density from the droplet temperature increasing during the transition, with evaporation of the droplet. The plateau is evident for the 10% mixture and to a lesser degree for the 20% mixture. While JP8 itself is a highly multicomponent blend, preferential evaporation is not evident from the trends reported previously (*8*), indicating that with so many components in JP8 many are evaporating simultaneously to eliminate the distinction between components. The con-

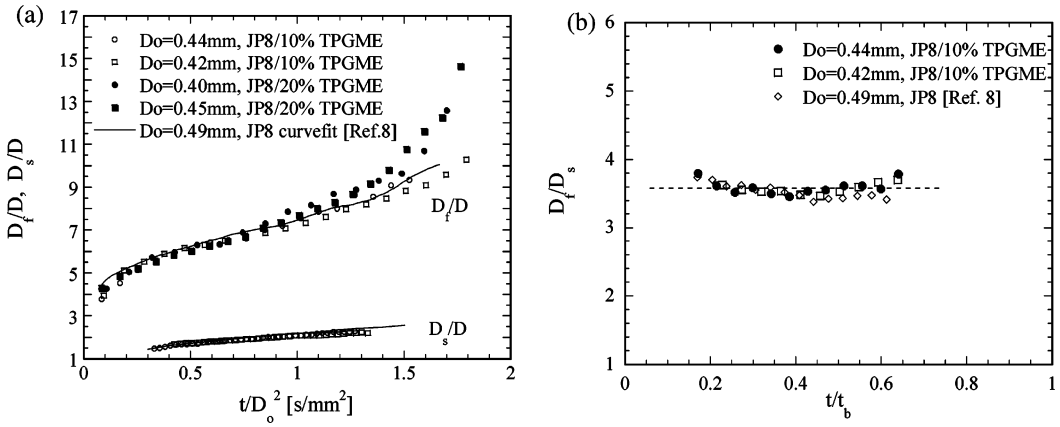

FIGURE 7. (a) Evolution of flame and soot shell standoff ratios for both JP8/TPGME (10% and 20%) mixture droplets burning in air. (b) Ratio of the flame to soot shell diameters with time scaled by the droplet burning lifetime. There are no D_s measurements for JP8/20% TPGME in (a) because the soot shell was not clearly articulated for this mixture (see Figure 3).

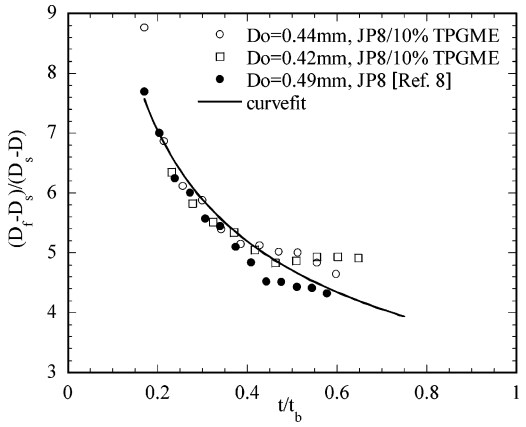

FIGURE 8. Scaling of three characteristic diameters with time normalized by the droplet burning lifetime.

centration of TPGME in JP8 is far higher than that of any other single constituent in JP8, so one may view the JP8/TPGME blend more like a binary mixture of constituents with different boiling points and volatilities. Figure 6 lends support to this interpretation. For significant differences in boiling points of binary mixture droplets, the plateau can be quite pronounced (*27*).

Figure 7a shows the evolution of the flame and soot standoff ratios. Only data for the 10% mixture are shown because at 20% TPGME the soot shell was all but eliminated as shown in Figure 3. From Figure 7a, $1 < D_s/D < D_f/D$, which follows because soot forms on the fuel side of the flame. With soot forming on the fuel-rich side of the flame, and the flame largely dictating the temperature gradient, soot aggregate trapping is expected to track with the flame front. This point is more clearly seen in Figure 7b, which shows that D_f/D_s is essentially constant throughout burning for JP8 and JP8/TPGME blends.

The 10% TPGME mixture has an evolution of flame standoff ratio almost identical to that of JP8 as shown in Figure 7b, whereas the 20% TPGME mixture has a slightly higher ratio than JP8 at the late burning regime due to faster burning. The flame standoff ratio increases continuously as burning progresses, which is due to fuel vapor accumulation early on (*38*). Figure 7a also shows that the soot standoff positions are virtually indistinguishable between JP8 and the 10% TPGME mixture. Furthermore, while D_s/D tracks with D_f/D, D_s/D shows a weaker dependence on time because of the inertia of the soot aggregates, which makes them less responsive to thermal and dynamic changes in the surrounding gas.

Correlation. The values of D, D_f, and D_s are linked by the radial convection field, the temperature gradient from the droplet surface to the flame, and the forces acting on the soot aggregates which depend on these fields. A relationship among the variables was previously presented as (*8*)

$$\frac{D_f - D_s}{D_s - D} = C\left(\frac{t}{t_b}\right)^n \qquad (2)$$

where t is the time, t_b is the droplet lifetime, and C and n are empirical fitting coefficients. According to eq 2, data plotted as $(D_f - D_s)/(D_s - D)$ vs t/t_b would fall on a single curve. Figure 8 shows that this is in fact the case for JP8 and a 10% JP8/TPGME mixture. The solid line comes from eq 2 and was derived from JP8 and JP8 + 10% TPGME data. Note that, for JP8 + 20% TPGME, the soot shell diameter could not be measured due to the significant reduction of soot formation and accumulation (see Figure 3c), so there are no data for the 20% mixture in Figure 8 (e.g., Figure 7a). The line in Figure 8 is a best fit using eq 2 with $C = 3.47$ and $n = -0.44$ for this data set. The utility of a correlation such as eq 2 is that it allows a prediction of D_s given the droplet and flame diameters for this complex blend.

Acknowledgments

We thank Dr. Edward Owens of Southwest Research Institute (San Antonio, TX) for supplying the JP8 and TPGME used in this study, as well as for helpful discussions. Assistance with the experiments by Messrs. Daniel Catropa, Radford Fagan, and Darius Liu is acknowledged. We also benefited from helpful discussions with Dr. Wing Tsang of the National Institute of Standards and Technology. This research was supported by the National Aeronautics and Space Administration through Grant NAG 3-2224 with Dr. Merril King as Program Director and Dr. Daniel Dietrich as Project Monitor.

Literature Cited

(1) Edwards, T.; Maurice, L. Q. *J. Propul. Power* **2001**, *17* (2), 461−466.
(2) Mayfield, H. T. *JP-8 Composition and Variability*; AL/EQ-TR-1996-0006; 1996.
(3) Edwards, T. *J. Propul. Power* **2003**, *19* (6), 1089−1107.
(4) *Workshop on Combustion Simulation Databases for Real Transportation Fuels*, Sept 4−5, 2003; Tsang, W., Ed.; Report No. NIST-IR-7155; National Institute of Standards and Technology: Gaithersburg, MD, 2003.
(5) *Handbook of Aviation Fuel Properties*; Coordinating Research Council Report No. 530; Coordinating Research Council: Alpharetta, GA, 1983.
(6) Heneghan, S. P.; Zabarnick, S.; Ballal, D. R.; Harrison, W. E. *J. Energy Resour. Technol.* **1996**, *118*, 170−179 (see also AIAA Paper 96-0403).
(7) Heneghan, S. P.; Williams, T. F.; Martel, C. R.; Ballal, D. R. *J. Eng. Gas Turbines Power* **1993**, *115*, 480−484.
(8) Bae, J. H.; Avedisian, C. T. *Combust. Flame* **2004**, *137*, 148−162.
(9) Imschweiler, D.; McKeand, M.; Lee, S. Y.; Saretto, S.; Linevsky, M.; Litzinger, T. A.; Santoro, R. J. AIAA 2003-5088; July 2003.
(10) González D., M. A.; Piel, W.; Asmus, T.; Clark, W.; Garbak, J.; Liney, E.; Natarajan, M.; Naegeli, D. W.; Yost, D.; Frame, E. A.; Wallace, J. P., III. SAE Technical Paper Series No. 2001-01-3632; Society of Automotive Engineers: Warrendale, PA, 2001.
(11) Miyamoto, N.; Ogawa, H.; Nurun, N. M.; Obata, K.; Arima, T. SAE Technical Paper Series No. 980506; Society of Automotive Engineers: Warrendale, PA, 1998.
(12) Curran, H. J.; Fisher, E. M.; Glaude, P. A.; Marinov, N. M.; Pitz, W. J.; Westbrook, C. K.; Layton, D. W.; Flynn, P. F.; Durrett, R. P.; zur Loye, A. O.; Akinyemi, O. C.; Dryer, F. L. SAE Technical Paper Series No. 2001-01-0653; Society of Automotive Engineers: Warrendale, PA, 2001.
(13) González D., M. A.; Natarajan, M.; Clark, W.; Yost, D.; Frame, E. A.; Wolf, L. R.; Kenney, T. E.; Ball, J. C.; Garbak, J. A.; Wallace, J. P., III; Wright, K. J.; Hilden, D. L.; Eng, K. D. SAE Technical Paper Series No. 2002-01-2884; Society of Automotive Engineers: Warrendale, PA, 2002.
(14) Mueller, C. J.; Pitz, W. J.; Pickett, L. M.; Martin, G. C.; Siebers, D. L.; Westbrook, C. K. SAE Technical Paper Series No. 2003-01-1791; Society of Automotive Engineers: Warrendale, PA, 2003.
(15) Glassman, I. *Proc. Combust. Inst.* **1988**, *22*, 295−311.
(16) Megaridis, C. M.; Dobbins, R. A. *Combust. Sci. Technol.* **1989**, *66*, 1−16.
(17) Dobbins, R. A. *Combust. Flame* **2002**, *130*, 204−214.
(18) Glassman, I. *Combustion*, 3rd ed.; Academic Press: San Diego, CA, 1996; pp 285−308 and 417.
(19) Yang, J. C.; Jackson, G. S.; Avedisian, C. T. *Proc. Combust. Inst.* **1990**, *23*, 1619−1625.
(20) Natarajan, M.; González, D. M. A.; Frame, E. A.; Naegeli, D. W.; Liney, E.; Asmus, T.; Piel, W.; Clark, W.; Wallace, J. P., III; Garbak, J. SAE Technical Paper Series No. 2001-01-3631; Society of Automotive Engineers: Warrendale, PA, 2001.
(21) Avedisian, C. T. In *Physical and Chemical Aspects of Combustion*; Dryer, F. D., Sawyer, R. F., Eds.; Combustion Science & Technology, Gordon & Breach Publishers: Amsterdam, The Netherlands, 1997; Vol. 4, pp 135−160.
(22) Ben-dor, G.; Elberin, T.; Krasovitov, B. *Proc. R. Soc. London, A* **2003**, *459*, 677−703.

(23) Jackson, G. S.; Avedisian, C. T. *Combust. Sci. Technol.* **1996**, *115*, 125−149.
(24) Marchese, A. J.; Dryer, F. L.; Nayagam, V. *Combust. Flame* **1999**, *116*, 432−459.
(25) Kumar, S.; Ray, A.; Kale, S. R. *Combust. Sci. Technol.* **2002**, *174* (9), 67−102.
(26) Jackson, G. S.; Avedisian, C. T.; Yang, J. C. *Proc. R. Soc. London, A* **1991**, *435*, 359−368.
(27) Jackson, G. S.; Avedisian, C. T. *Int. J. Heat Mass Transfer* **1998**, *41* (16), 2503−2515.
(28) Sirignano, W. A. *Fluid Dynamics and Transport of Droplets and Sprays*; Cambridge University Press: New York, 1999; pp 7, 16−18, and 120−123.
(29) Jackson, G. S.; Avedisian, C. T.; Yang, J. C. *Int. J. Heat Mass Transfer* **1992**, *35* (8), 2017−2033.
(30) Jackson, G. S.; Avedisian, C. T. *Proc. R. Soc. London, A* **1994**, *446*, 255−276.
(31) Avedisian, C. T.; Yang, J. C.; Wang, C. H. *Proc. R. Soc. London, A* **1988**, *420*, 183−200.
(32) Avedisian, C. T. *J. Propul. Power* **2000**, *16* (4), 628−635.
(33) Bae, J. H. Ph.D. Thesis, Sibley School of Mechanical and Aerospace Engineering, Cornell University, Ithaca, NY, 2005.
(34) Avedisian, C. T.; Callahan, B. J. *Proc. Combust. Inst.* **2000**, *28*, 991−997.
(35) Mikami, M.; Oyagi, H.; Kojima, N.; Kikuchi, M.; Wakashima, Y.; Yoda, S. *Combust. Flame* **2005**, *141*, 241−252.
(36) Avedisian, C. T.; Jackson, G. S. *J. Propul. Power* **2000**, *16* (6), 974−979.
(37) Manzello, S. L.; Choi, M. Y. *Int. J. Heat Mass Transfer* **2002**, *45*, 1109−1116.
(38) Law, C. K.; Chung, S. H.; Srinivasan, N. *Combust. Flame* **1980**, *38*, 173−198.

Received for review September 21, 2004. Revised manuscript received June 15, 2005. Accepted June 17, 2005.

ES048516W